



OPEN

Triazolopyrimidine herbicides are potent inhibitors of *Aspergillus fumigatus* acetohydroxyacid synthase and potential antifungal drug leads

Y. S. Low¹, M. D. Garcia¹, T. Lonhienne¹, J. A. Fraser^{1,2}, G. Schenk¹ & L. W. Guddat^{1✉}

Aspergillus fumigatus is a fungal pathogen whose effects can be debilitating and potentially fatal in immunocompromised patients. Current drug treatment options for this infectious disease are limited to just a few choices (e.g. voriconazole and amphotericin B) and these themselves have limitations due to potentially adverse side effects. Furthermore, the likelihood of the development of resistance to these current drugs is ever present. Thus, new treatment options are needed for this infection. A new potential antifungal drug target is acetohydroxyacid synthase (AHAS; EC 2.2.1.6), the first enzyme in the branched chain amino acid biosynthesis pathway, and a target for many commercial herbicides. In this study, we have expressed, purified and characterised the catalytic subunit of AHAS from *A. fumigatus* and determined the inhibition constants for several known herbicides. The most potent of these, penoxsulam and metosulam, have K_i values of 1.8 ± 0.9 nM and 1.4 ± 0.2 nM, respectively. Molecular modelling shows that these compounds are likely to bind into the herbicide binding pocket in a mode similar to *Candida albicans* AHAS. We have also shown that these two compounds inhibit *A. fumigatus* growth at a concentration of 25 μ g/mL. Thus, AHAS inhibitors are promising leads for the development of new anti-aspergillosis therapeutics.

Aspergillosis is an invasive fungal disease caused by members of the genus *Aspergillus*. *A. fumigatus* makes up 90% of such infections, and in immunocompromised patients these can prove to be debilitating and potentially fatal¹. Azoles such as voriconazole and itraconazole are the first choice of drugs for treatment, but options are limited due to commonly occurring side effects (e.g. liver toxicity and neuropathy)^{2,3}. In addition, the effectiveness of the currently available drugs is being impeded by the emergence of drug-resistant strains³. This is especially true in the recent COVID-19 pandemic, where a hybrid *Aspergillus* species, *Aspergillus latus*, was isolated from COVID-19 patients and found to have increased drug resistance compared to its parental strains⁴. These issues highlight the urgent need for alternative or more effective treatments for aspergillosis infections.

A potential new antifungal drug target is acetohydroxyacid synthase (AHAS; EC 2.2.1.6), the first enzyme in the branched chain amino acids (BCAA) biosynthesis pathway. Fungal pathogens *Candida albicans* and *Cryptococcus neoformans*, whose AHAS genes have been knocked out, are auxotrophic for isoleucine and valine, and are no longer virulent in infected mice^{5,6}. Inhibition of AHAS therefore shuts down the BCAA biosynthesis pathway and prevents protein synthesis, and ultimately stops the growth of these fungal pathogens in mice^{5,6}. It is also noteworthy that AHAS and the BCAA pathway are absent in animals and humans. Therefore, inhibitors that are designed to target AHAS are likely to be harmless to these species.

AHAS inhibitors have previously been developed into commercial herbicides^{7,8}. There are now over 50 such commercial herbicides across five different chemical families, namely the sulfonyleureas, triazolopyrimidines, sulfonylamino-carbonyl-triazolinones, pyrimidyl(oxy/thio)benzoates and imidazolinones (Fig. 1). These herbicides have been used with great efficacy for crop protection worldwide, and importantly exhibit low toxicity toward animals⁹. AHAS inhibition by herbicides follows an elaborate process where two mechanisms are involved. Beside direct inhibition of enzyme activity, most herbicides are able to trigger the oxidative inactivation

¹School of Chemistry and Molecular Biosciences, The University of Queensland, Brisbane, QLD 4072, Australia. ²Australian Infectious Diseases Research Centre, The University of Queensland, Brisbane, QLD 4072, Australia. ✉email: luke.guddat@uq.edu.au

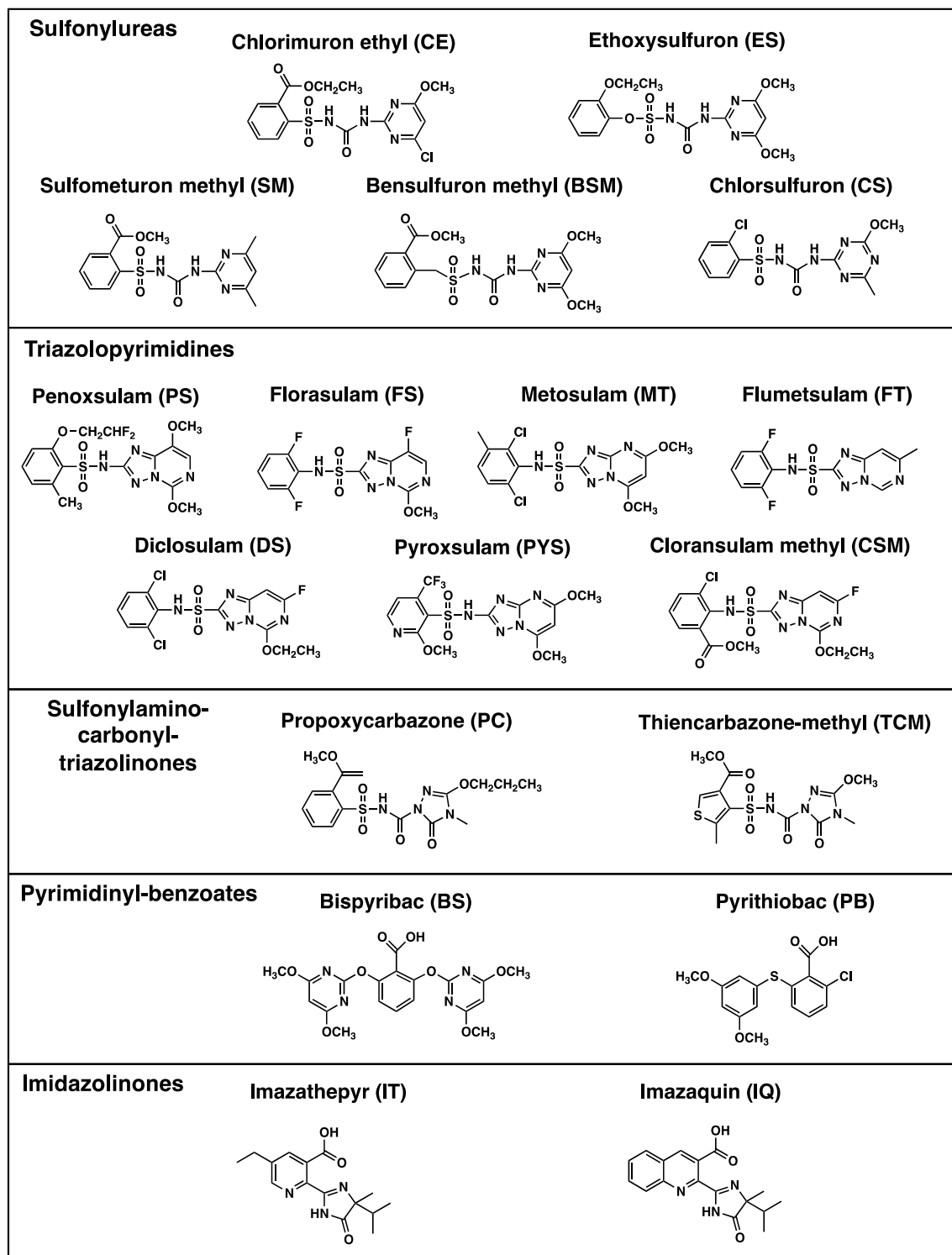


Figure 1. Chemical structures of the commercial herbicides evaluated here. A general feature of the sulfonylureas, triazolopyrimidines, and sulfonylamino-carbonyl-triazolinones is the presence of both an aromatic and a heterocyclic ring. The structural images were created using CHEMDRAW 20.0.

of the enzyme in a process referred to as “time-dependent accumulative inhibition”^{10,11}. The latter process is an important contributor to the potent herbicidal^{10,12} and anti-fungal^{13,14} activity exhibited by these compounds.

Here it is suggested that these herbicides could also possess anti-aspergillosis activity. In support of this hypothesis, several AHAS inhibitors have been shown to inhibit the growth of human fungal pathogens in culture and in mice^{13,14}. Indeed, members of the sulfonylurea family of herbicides can inhibit *C. albicans* AHAS (CaAHAS) and *C. albicans* growth¹⁴. In addition, a novel series of triazolopyrimidines also possesses antifungal

properties against *A. fumigatus* grown in culture (although these compounds were not directly tested as AHAS inhibitors)¹⁵. In this study, we expressed, purified and characterised the catalytic subunit of recombinant *A. fumigatus* AHAS (*Afu*AHAS) and evaluated the inhibitory properties of commercial herbicides from all five chemical families. We also assessed the effectiveness of these compounds on *Aspergillus* cell growth in culture, demonstrating their potential as drug leads to combat aspergillosis.

Results and discussion

Protein expression and purification. *Afu*AHAS was recombinantly expressed (see “Materials and methods”), and purified by IMAC (Fig. 2a) and size exclusion chromatographies (Fig. 2b). SDS-PAGE showed a protein of ~75 kDa (Fig. 2c), in good agreement with the calculated molecular mass (72 kDa) of the *Afu*AHAS catalytic subunit.

Characterisation of *Afu*AHAS. The catalytic activity of *Afu*AHAS using pyruvate as a substrate was determined by the continuous method. The data were fitted using the Michaelis–Menten equation ($R^2 = 0.97$, Fig. 2d). The K_M for pyruvate for *Afu*AHAS is 17.32 ± 1.97 mM, and the k_{cat} is 3.29 ± 0.10 s⁻¹. When comparing these kinetic parameters to that of *Ca*AHAS (K_M : 2.6 ± 0.1 mM, k_{cat} : 3.75 ± 0.13 s⁻¹)¹⁴ and *Sc*AHAS (K_M : 3.6 ± 0.6 mM, k_{cat} : 2.4 ± 0.25 s⁻¹)^{14,16}, the K_M of *Afu*AHAS is ~four to six fold higher, suggesting the active site structure and response to substrate binding are not identical. The varying K_M values may be attributed to the sequence differences in the catalytic Q-loop, whose presence is necessary for catalysis to occur (Fig. 2e). Further insights on the structure and dynamics of the active sites during catalysis will be required to understand the effects of these differences.

In order to determine the number of subunits in *Afu*AHAS, size exclusion chromatography (SEC) followed by multi-angle light scattering (MALS) was performed (Fig. 2f). From the MALS analysis, the 1, 5, and 10 mg/mL samples have molecular masses of 171.7, 202.7 and 268.8 kDa, respectively. The value of 268.8 kDa is consistent with the theoretical molecular mass for a tetramer of 288.3 kDa. These results suggest that at higher enzyme concentrations, *Afu*AHAS is predominantly tetrameric, but upon dilution the presence of lower molecular weight forms (e.g. dimeric proteins) becomes more relevant. Previous studies have shown that the catalytic subunits of *Saccharomyces cerevisiae* AHAS crystallize as dimer¹⁷, while *A. thaliana* and *C. albicans* AHAS catalytic subunits crystallize as tetramers^{13,18}. However, in general AHAS complexes adopt the shape of a Maltese cross where the active form of the CSU is dimeric¹⁹. This suggests that the tetrameric form of the catalytic subunit observed at higher concentrations in *A. thaliana* and *C. albicans* crystal structures^{12,13,18}, and here through SEC-MALS of *Afu*AHAS, may not represent a physiologically active form of the enzyme.

K_i values of commercial herbicides for *Afu*AHAS. The herbicide binding stoichiometry of *Afu*AHAS was investigated by measuring the activity of increasing concentrations *Afu*AHAS in the absence and presence of 0.5 μ M of the sulfonylurea, chlorimuron ethyl (CE; Fig. 1). The results show that 0.5 μ M CE can fully inhibit 1.06 μ M of *Afu*AHAS (Fig. 3a), giving a 1:2 inhibitor to enzyme ratio, which has also been observed in other AHAS studies¹⁰. Thus, once one active site is blocked, communication is halted and the second active site is no longer capable of substrate turnover²⁰.

Eighteen commercial herbicides from five chemical families (Fig. 1) were tested for their ability to inhibit *Afu*AHAS. In order to accurately determine the K_i values of herbicides for *Afu*AHAS, a partial anaerobic environment was established through nitrogen bubbling of the assay buffer in the presence of 2-mercaptoethanol (see “Materials and methods”, Supplementary Fig. 2)¹².

The K_i values of the herbicides for *Afu*AHAS under these conditions are listed in Table 1. Among the five chemical families, the triazolopyrimidines generally have the highest affinity. PS and MT have the lowest K_i values of 1.8 ± 0.92 nM and 1.4 ± 0.18 nM, respectively (Fig. 3b). For the triazolopyrimidine family there is a strong correlation in K_i values for *Afu*AHAS and *Ca*AHAS (Table 1), suggesting the herbicides of this family have very similar binding modes in the two enzymes (discussed below).

Amongst the sulfonylureas, CE has the lowest K_i (23.4 ± 1.3 nM), while the other sulfonylureas studied here have K_i values in the range from 220 to 3100 nM (Table 1). Relative to *Ca*AHAS, the sulfonylureas bind to *Afu*AHAS with an increase in K_i of ~4–10-fold. For the sulfonylamino-carbonyl-triazolinones and pyrimidinylbenzoates, the herbicides have K_i values that are generally higher than those of the triazolopyrimidine and sulfonylurea families. Furthermore, the imidazolinones tested here show no inhibition of *Afu*AHAS at concentrations up to 100 μ M, whilst they weakly inhibit *Ca*AHAS. Overall, however, there is a good correlation of the K_i values between families and between the two enzymes (Fig. 3c).

Accumulative inhibition by the commercial herbicides on *Afu*AHAS. Accumulative inhibition of *Afu*AHAS was evaluated through the determination of the apparent first-order rate constants of enzyme inactivation (k_{iapp}) and enzyme recovery (k_3)¹¹, and the efficiency of accumulative inhibition, k_{iapp}/k_3 ¹³ (Table 1). Among all the herbicides, the members of the triazolopyrimidine family were generally shown to be most efficient accumulative inhibitors of *Afu*AHAS (Table 1). In particular, PS and MT have the most potent time-dependent inhibition (k_{iapp}/k_3 values of 1426 and 1750, respectively), reflected by the high k_{iapp} of accumulative inhibition and the relatively low rate of enzyme recovery (k_3) (Table 1). PS has a ~four-fold higher rate of enzyme inactivation compared to MT. However, due to its ~five-fold lower enzyme recovery rate, stronger accumulative inhibition is achieved by MT over time (Fig. 3d). Comparison of the k_{iapp} and k_3 values for PS and MT in *Afu*AHAS and *Ca*AHAS show that the k_{iapp} values are similar between the two enzymes (*Afu*AHAS k_{iapp} : 18.5 min⁻¹ (PS), 4.2 min⁻¹ (MT); *Ca*AHAS k_{iapp} : 15.26 min⁻¹ (PS), 3.39 min⁻¹ (MT)¹³), while the k_3 values are ~five to ten-fold lower in *Afu*AHAS for PS and MT, respectively (*Afu*AHAS k_3 : 0.013 min⁻¹ (PS), 0.0024 min⁻¹ (MT); *Ca*AHAS

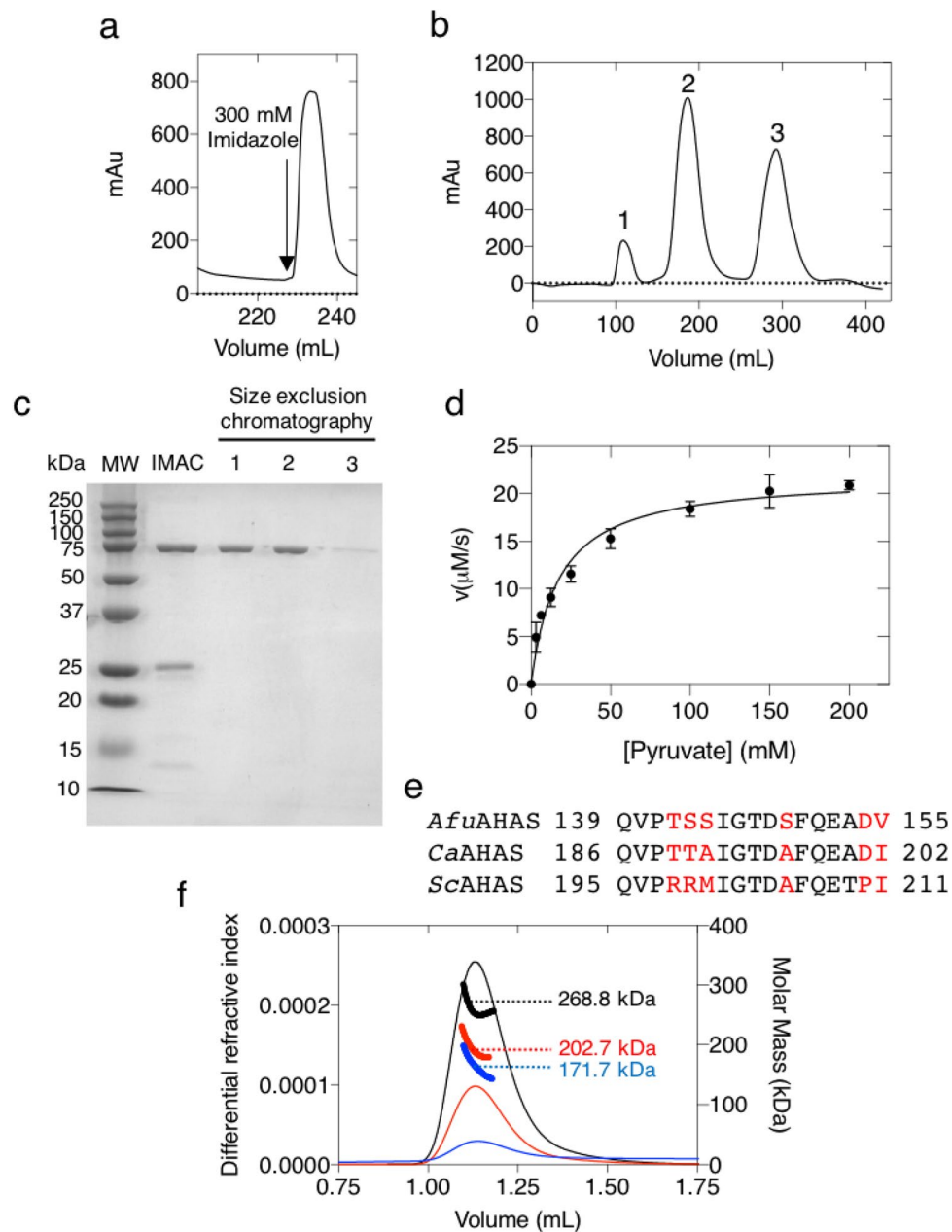


Figure 2. Purification of *AfuAHAS* and determination of its quaternary structure. **(a)** IMAC purification from cell lysate. **(b)** Size exclusion chromatography of the IMAC eluate using a Sephacryl-200-HR column (Pharmacia). Peak 1 corresponds to the void volume. Peak 2 has enzymatic activity. Peak 3 represents the cofactor salts. **(c)** Cropped SDS-PAGE for the purification of *AfuAHAS*. MW Molecular weight marker, IMAC eluate; Lanes 1, 2 and 3 correspond to peaks 1, 2 and 3 of the size exclusion chromatogram. See Supplementary Fig. 1 for uncropped version. **(d)** Pyruvate saturation curve for *AfuAHAS*. The data (measured in triplicate) were obtained using a continuous spectrophotometric method. The solid curve shows the best fit to the Michaelis–Menten equation with an R^2 value of 0.97. **(e)** Comparison of the Q-loop sequences in the catalytic subunit between *AfuAHAS*, *CaAHAS* and *ScaAHAS*. **(f)** SEC-MALS of peak 2 at three different loading concentrations (1, 5, 10 mg/mL, in blue, red and black, respectively) using a Superdex 200 Increase 5/150 GL column. The MALS data were processed using the ASTRA software (Wyatt Technology).

k_3 : 0.074 min^{-1} (PS), 0.023 min^{-1} (MT)¹³. Consequently, the accumulative inhibitory efficiencies of PS and MT for *CaAHAS* (k_{iapp}/k_3 : 206 and 147.4 for, respectively¹³) are approximately one order of magnitude smaller than for *AfuAHAS*. Thus, taking into account both the corresponding K_i values and accumulative inhibition, PS and MT are more potent inhibitors of *AfuAHAS* than *CaAHAS*.

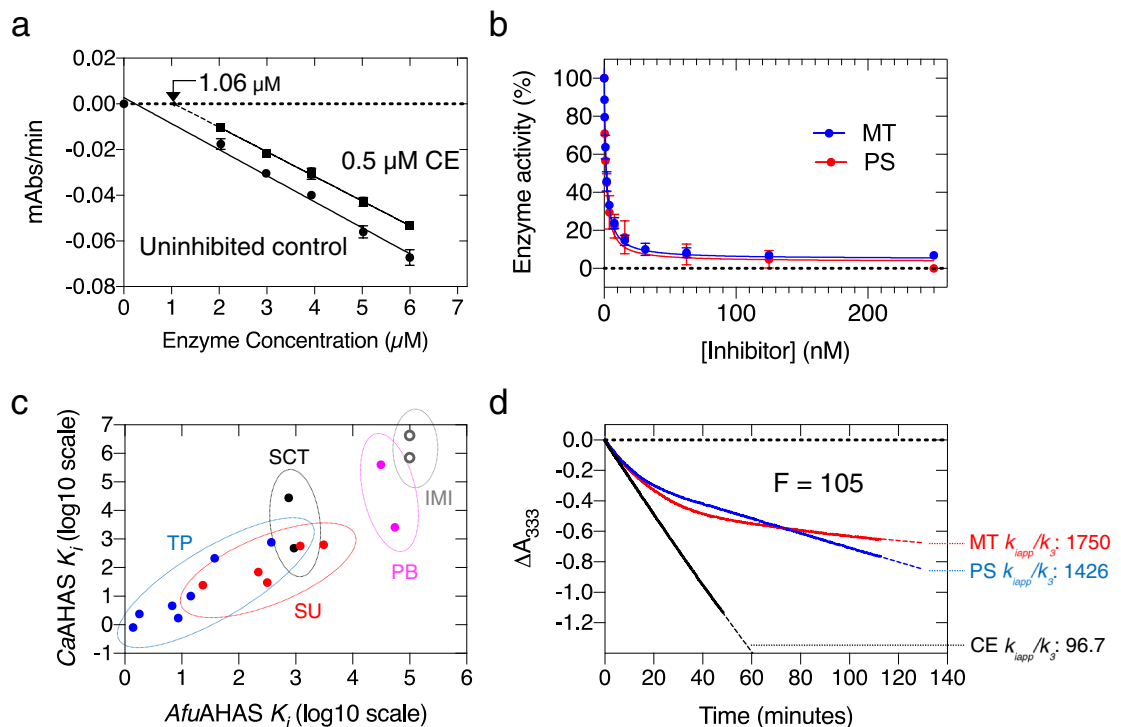


Figure 3. Inhibition of *AfuAHAS* by commercial herbicides. **(a)** Measurement of *AfuAHAS* activity in the presence and absence of 0.5 μM CE to determine herbicide binding stoichiometry. Extrapolation of the linear regression line (dashed line) showed that 1.06 μM of enzyme was fully inhibited by 0.5 μM CE. **(b)** *AfuAHAS* catalytic activity vs. inhibitor concentration. The data were fitted using Eq. (1) (see “Materials and methods”) for tight binding inhibitors. **(c)** Correlation of K_i values between *AfuAHAS* and *CaAHAS* for the five AHAS herbicide families. TP: Triazolopyrimidines, SU: Sulfonylureas, SCT: Sulfonylamino-carbonyl-triazolinones, PB: Pyrimidinyl-benzoates, IMI: Imidazolinones. **(d)** Accumulative inhibition curves for PS, MT and CE. The data were fitted using Eq. (3) (dashed line). For a direct comparison of the strength of accumulative inhibition, the F value (free enzyme/enzyme-inhibitor complex ratio) was set to 105 for the three inhibitors. The data show that MT is the most potent accumulative inhibitor. Images were created using GraphPad Prism 7.01.

Analysis of herbicide binding in *AfuAHAS*. Analysis of *AfuAHAS*, *S. cerevisiae* AHAS (*ScAHAS*), *CaAHAS*, *C. neoformans* AHAS (*CnAHAS*) and *AtAHAS* catalytic subunit sequences shows that most of the herbicide binding site residues are highly conserved amongst these AHASs (Fig. 4). The exceptions are S254 and S259 in *AfuAHAS*, which are hydrophobic residues in the other fungal and plant AHASs, as well as A719, which is a glycine or serine in *ScAHAS* and *AtAHAS*, respectively (Fig. 4). The conservation of herbicide binding site residues in *AfuAHAS* and *CaAHAS* is consistent with the correlation found in the K_i values (Fig. 3c). Attempts to crystallize *AfuAHAS*, either in the presence or absence of inhibitors were not successful, so molecular modelling and docking was used to provide structural explanations for the inhibition results. A homology model of *AfuAHAS* was generated using SWISS-MODEL²¹ and the crystal structures of *CaAHAS* with bound herbicides were used to identify herbicide interactions in *AfuAHAS* (Fig. 5). The homology model has an rmsd of 0.368 Å for 1196 out of 1231 Ca atoms after superimposition with *CaAHAS*. In total, 95.7% of the amino acid residues have favourable Ramachandran dihedral angles and there are 0.4% outliers. The modelling shows that the herbicide binding site structures in *CaAHAS* and the *AfuAHAS* model are similar (Fig. 5a–c). The most significant differences are A191 and A196 in *CaAHAS* which are replaced by serine (*i.e.* S254 and S259; Figs. 4 and 5).

Based on the published *CaAHAS* structures, A191 and A196 form hydrophobic interactions with the aromatic ring (Fig. 1) of the herbicides (Fig. 5)¹³. Inhibitor docking with the *AfuAHAS* model shows little change in the distances of S254 and S259 to the bound herbicide compared to A191 and A196 in *CaAHAS* (Fig. 5). The proximity of the serine residues to the bound herbicides remain sufficient for hydrophobic contacts to occur. The change in K_i values (Table 1) observed when sulfonylureas and sulfonylamino-carbonyl-triazolinones bind could be the result of the subtle changes to the herbicide binding site in *AfuAHAS*, *e.g.* the serine residues might promote binding of an ordered water molecule, thereby modifying the binding mode of the inhibitors. However, for PS and MT these sequence changes have no apparent effect on binding.

The presence of S254 and S259, not observed in the other pathogenic fungi and *A. thaliana*, could provide a target for the design of specific *A. fumigatus* inhibitors. Introducing hydrophilicity into the aromatic ring structure of the herbicide to form hydrogen bonds with the serine residues may potentially improve inhibitor binding affinity.

Herbicide	K_i (nM)	K_i for CaAHAS (nM)*	k_{iapp} (min ⁻¹)	k_3 (min ⁻¹)	k_{iapp}/k_3
Sulfonylureas					
CE	23.4 ± 1.3	24.3 ± 2.5	0.6 ± 0.1	0.006	96.7
ES	220 ± 11	69.3 ± 6.9	1.0 ± 0.3	0.031	31.3
SM	3100 ± 0.5	630 ± 51	0.2 ± 0.1	0.0065	26.2
CS	1200 ± 0.2	570 ± 59	NAI	NAI	–
BSM	316 ± 101	29.9 ± 2.7	0.7 ± 0.1	0.0026	257.7
Imidazolinones					
IQ	> 10 ⁵	716,000 ± 61,000	ND	ND	–
IT	> 10 ⁵	4.3 ± 0.7 × 10 ⁶	ND	ND	–
Triazolopyrimidines					
PS	1.8 ± 0.9	2.4 ± 0.3	18.5 ± 2.6	0.013	1426
FS	14.4 ± 2.7	10.1 ± 1.7	17.8 ± 0.6	0.014	1268
MT	1.4 ± 0.2	0.8 ± 0.1	4.2 ± 0.6	0.0024	1750
FT	373 ± 70	773 ± 62	NAI	NAI	–
DS	8.7 ± 5.0	1.7 ± 0.8	3.2 ± 0.8	0.006	530
PYS	37.8 ± 1.5	212 ± 18	6.9 ± 0.4	0.05	138.8
CSM	6.8 ± 3.4	4.6 ± 1.2	8.7 ± 1.8	0.016	545
Sulfonylamino-carbonyl-triazolinones					
PC	937 ± 460	484 ± 37	0.34 ± 0.09	0.03	11.3
TCM	752 ± 86	28,000 ± 6000	0.59 ± 0.03	0.011	53.6
Pyrimidinyl-benzoates					
BS	55,000 ± 1400	2600 ± 300	NAI	NAI	–
PB	31,100 ± 2000	403,000 ± 37,000	NAI	NAI	–

Table 1. Apparent first-order rate of inhibition (k_{iapp}), first-order rate of enzyme recovery (k_3), and inhibition constants (K_i) of the commercial herbicides for *Afu*AHAS. * K_i values for *Ca*AHAS are shown for comparison were obtained from Garcia et al.¹³. NAI No reversible accumulative inhibition observed, ND Not determined. See Fig. 1 for chemical structures of compounds.

<i>A. fumigatus</i>	172	YPGGAIL	...	246	FCGQVPTSSIGTDSFQEADV	...	307	DLPKDIT	...	412	MLGMHGS	...
<i>C. albicans</i>	109	YAGGAIL	...	183	FSGQVPTTAIGTDAFQEADI	...	244	DLPKDVT	...	347	MLGMHGS	...
<i>S. cerevisiae</i>	115	YPGGAIL	...	187	FTGQVPTSAIGTDAFQEADV	...	248	DLPKDVT	...	351	MLGMHGC	...
<i>C. neoformans</i>	149	YPGGAIL	...	221	FCGQVATNLIGSDAFQEADV	...	282	DLPKDVT	...	393	MIGMHGS	...
<i>A. thaliana</i>	120	YPGGASM	...	192	ITGQVPRRMIGTDAFQETPI	...	253	DVPKDIQ	...	351	MLGMHGT	...
<i>A. fumigatus</i>	435	GARFDDRVVTGN	...	638	NNEEQGMVTQWQNLFY	...	715	PMVPAGSAL	...	752		
<i>C. albicans</i>	370	GARFDDRVVTGN	...	572	NNEEQGMVTQWQSLFY	...	649	PMVPAGKAL	...	683		
<i>S. cerevisiae</i>	374	GARFDDRVVTGN	...	576	NNEEQGMVTQWQSLFY	...	653	PMVAGGSSL	...	687		
<i>C. neoformans</i>	416	GVRFDDRVVTGK	...	618	NNEFQGMVEQWQDLFY	...	696	PMIPAGKAL	...	718		
<i>A. thaliana</i>	371	GVRFDDRVVTGK	...	564	NNQHLGMVMQWEDRFY	...	649	PMIPSGGTF	...	670		

Figure 4. Partial alignment of four fungal and one plant AHAS sequences highlighting the herbicide binding site residues. The conserved residues are in green, while the variants are in red.

Minimum inhibitory concentration of *Aspergillus* sp. Lee et al. have shown that sulfonylurea herbicides have antifungal activity that reduces the growth of *C. albicans* in culture, while Garcia et al. have shown that CE can reduce *C. albicans* growth in infected mice^{13,14}. In this study, the minimal inhibitory concentration (MIC) of the herbicides on the cell growth was determined for four pathogenic *Aspergillus* species²³, *A. fumigatus*, *A. nidulans*, *A. niger*, *A. flavus*. The results show that CE, PS and MT inhibit the growth of *A. fumigatus* at 100, 25 and 25 µg/mL, respectively (Table 2). PS and MT also inhibit *A. nidulans* growth at 25 µg/mL. None of the other compounds tested showed activity at < 100 µg/mL, and the growth of *A. niger* and *A. flavus* is not impaired by any of the herbicides listed in Table 2.

The difference in susceptibility of the four *Aspergillus* species to the same herbicide (Table 2) may be attributed to a number of factors. However, comparison of the herbicide binding site residues between the different *Aspergillus* species (Fig. 6) show few differences, suggesting binding to the enzyme is not one of these. The lack of inhibitory activity on *A. niger* and *A. flavus* growth may be due to the production of proteins that manage oxidative stress, or differentially metabolize these herbicides (e.g. P_{450S})²⁴.

Richie et al. showed that *A. fumigatus* can scavenge BCAA from sheep blood, raising concerns on the efficacy of inhibiting the BCAA biosynthesis pathway for this fungus¹⁵. However, the primary route of *A. fumigatus* infection is through the lungs, where a porcine model has provided evidence that BCAA availability is limited in pulmonary secretions²⁵. *A. fumigatus* is thus unlikely to be able to scavenge sufficient BCAAs from the pulmonary

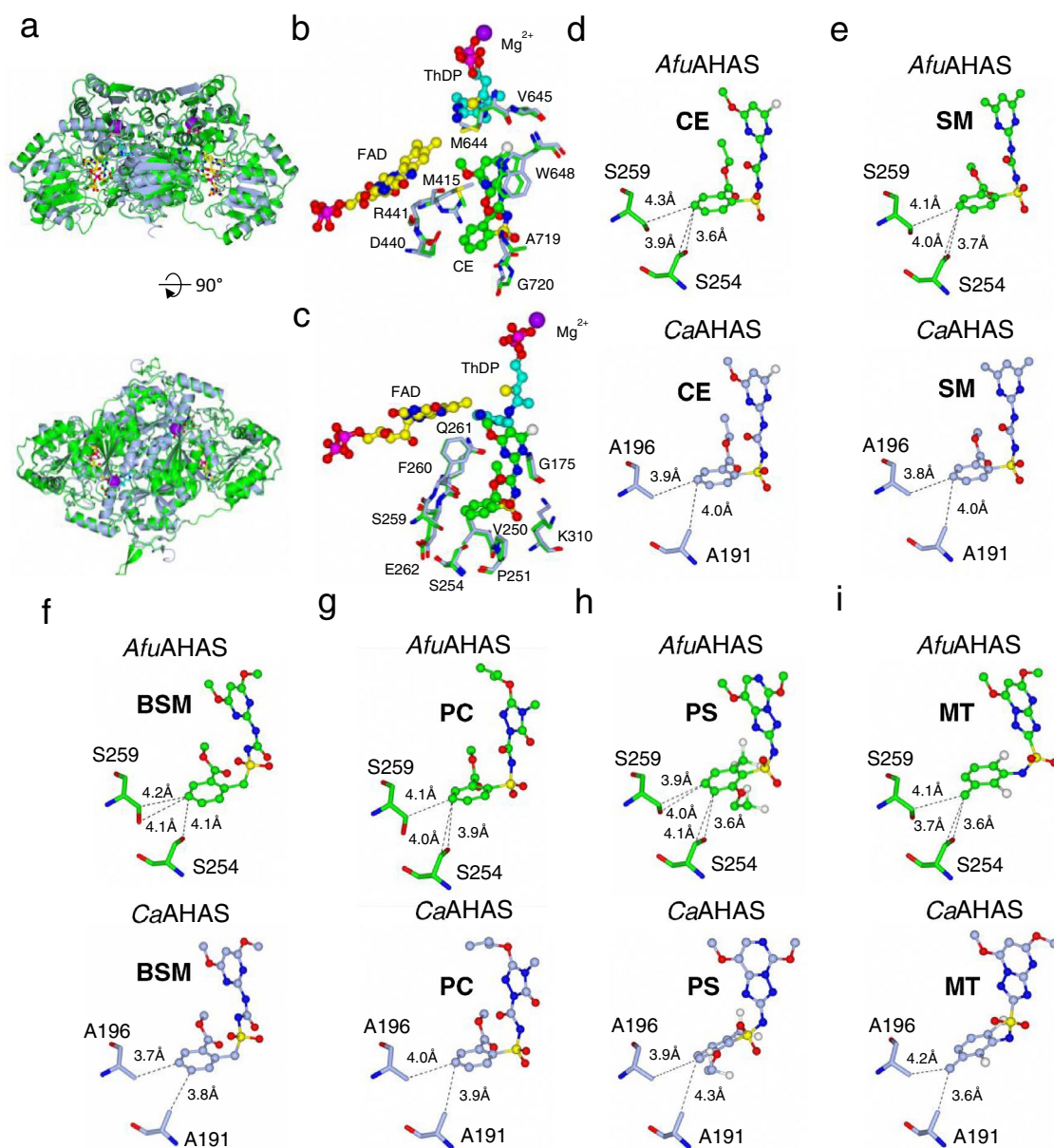


Figure 5. Structural comparisons of *AfuAHAS* and *CaAHAS*. **(a)** The overall structure of the *AfuAHAS* homology model (green) superimposed onto the crystal structure of *CaAHAS* (light blue). **(b, c)** The herbicide binding sites in *AfuAHAS* and *CaAHAS*. Residues that make up the binding site from the two different subunits are shown separately in panels **(b)** and **(c)**. **(d–i)** Comparison of CE, SM, BSM, PC, PS and MT binding to S254 and S259 in the *AfuAHAS* model and A191 and A196 of *CaAHAS* in the crystal structures (PDB IDs for the structures of the complexes are 6DEL, 6DEP, 6DEM, 6DES, 6DEQ and 6DER, respectively). The herbicides, thiamine diphosphate and flavin adenine dinucleotide are shown as ball and stick models with the carbon atoms in blue or green for the herbicides and protein and cyan and yellow for thiamine diphosphate and flavin adenine dinucleotide. The magnesium ions are shown as purple spheres. The amino acid side-chains are shown as stick models. The dashed lines represent distances between the two atoms, not necessarily bond formation. The images were prepared using CCP4mg²².

environment and would have to rely on *de novo* synthesis for growth. A biological assay that would closely mimic these conditions would provide a better estimate of the MIC values. In terms of potential toxicity, compounds of the triazolopyrimidine family have been shown to only be cytotoxic at concentrations at > 128 µg/mL on human blood and liver cell lines¹⁵. The MIC values of PS and MT are at least eight-fold lower than this concentration, suggesting that these herbicides have minimal cytotoxicity for human cells, and thus they are suitable drug leads.

Herbicide	<i>A. fumigatus</i>	<i>A. nidulans</i>	<i>A. niger</i>	<i>A. flavus</i>
	MIC (µg/mL) ^a			
Sulfonylureas				
CE	100	>100	>100	>100
ES	>100	>100	>100	>100
SM	>100	>100	>100	>100
CS	>100	>100	>100	>100
BSM	>100	>100	>100	>100
Triazolopyrimidines				
PS	25	25	>100	>100
FS	>100	>100	>100	>100
MT	25	25	>100	>100
FT	>100	>100	>100	>100
DS	>100	>100	>100	>100
PYS	>100	>100	>100	>100
CSM	>100	>100	>100	>100
Sulfonylamino-carbonyl triazolinones				
PC	>100	>100	>100	>100
TCM	>100	>100	>100	>100
Pyrimidinyl-benzoates				
BS	>100	>100	>100	>100
PB	>100	>100	>100	>100
Imidazolinones				
IT	>100	>100	>100	>100
IQ	>100	>100	>100	>100

Table 2. MIC values of herbicides for *A. fumigatus*, *A. nidulans*, *A. niger* and *A. flavus* cells. ^aMIC indicates concentration of herbicides in wells with no observable *Aspergillus* growth.

A. fumigatus 172 YPGGAIL ... 246 FCGQVPTSSIGTDSFQEADV ... 307 DLPKDIT ... 412 MLGMHGS ...
A. nidulans 110 YPGGAIL ... 184 FCGQVPTTSIGTDSFQEADV ... 245 DLPKDIT ... 350 MLGMHGS ...
A. niger 113 YPGGAIL ... 187 FCGQVPTSLIGTDSFQEADV ... 248 DLPKDIT ... 353 MLGMHGS ...
A. flavus 114 YPGGAIL ... 188 FCGQVPTSAIGTDSFQEADV ... 249 DLPKDIT ... 354 MLGMHGS ...

A. fumigatus 435 GARFDDRVTGN ... 638 NNEEQGMVTQWQNLFY ... 715 PMVPAGSAL ... 752
A. nidulans 373 GARFDDRVTGS ... 576 NNEEQGMVTQWQNLFY ... 653 PMVPGGSGSL ... 687
A. niger 376 GARFDDRVTGN ... 579 NNEEQGMVTQWQNLFY ... 656 PMVPAGCAL ... 690
A. flavus 377 GARFDDRVTGN ... 580 NNEEQGMVTQWQNLFY ... 657 PMVPAGSAL ... 691

Figure 6. Partial alignment of *A. fumigatus*, *A. nidulans*, *A. niger* and *A. flavus* AHAS sequences highlighting the herbicide binding site residues. Herbicide binding site residues are identified by red or green text to indicate variable or identical sequences, respectively.

Conclusion

Evaluation of the five chemical families of commercial herbicides show that the triazolopyrimidines have potent inhibitory properties against *Afu*AHAS. In particular, the herbicides PS and MT are tight binding inhibitors and also have strong accumulative inhibitory properties. These two herbicides are therefore good starting points for the design of novel antifungal compounds that target *Afu*AHAS. However, the bioavailability of the herbicide in *Aspergillus* cells needs to be improved for the design of more effective compounds that can prevent growth of this fungal pathogen.

Materials and methods

Preparation of *Afu*AHAS gene construct. The amino acid sequence for the catalytic subunit of *Afu*AHAS was obtained from the National Centre for Biotechnology Information (NCBI) (NCBI reference sequence: XP_754588.1). The construct was modified to remove the DNA coding for the first 111 amino acids belonging to the mitochondrial transit peptide sequence. An AUG start codon was added at the N-terminus of the peptide sequence. A Tobacco Etch Virus protease restriction site and a hexahistidine tag were added at the C-terminus of the peptide sequence. The gene sequence was synthesised in a pUC57 plasmid by Biomatik (Cambridge, Canada). The coding sequence for *Afu*AHAS was excised from the plasmid by *Hind*III/*Nde*I (New England Biolabs) digestion. The gene was then ligated with the pET30A(+) vector cut using the same restriction sites. *Escherichia coli* BL21 (DE3) cells were then transformed using the resultant pET30A(+)-*Afu*AHAS plasmid.

Protein expression and purification. All reagents were obtained from Sigma-Aldrich (St Louis, MO, USA) and were of analytical grade, unless otherwise stated. Protein expression and purification were performed as described previously for CaAHAS, but with some differences¹³. The gel filtration buffer used for size exclusion chromatography contains 10 mM potassium phosphate buffer pH 7.2, 300 mM NaCl, 10 μ M FAD and 1 mM DTT. The fractions containing the folded enzyme were pooled, and the potassium phosphate concentration was increased to 200 mM and 10 mM of MgCl₂ was added before concentration and storage at -80°C .

AfuAHAS assays. *Standard assays.* AHAS activity was measured in standard assay buffer containing 200 mM potassium phosphate buffer at pH 7.2, 10 mM MgCl₂, 1 mM ThDP, 10 μ M FAD and 100 mM pyruvate, at 30°C .

Two methods were used:

1. The continuous spectrophotometric method²⁶. The variation of absorbance at 333 nm wavelength was recorded (using a Shimadzu UV2550 UV/VIS spectrophotometer) to measure the disappearance of pyruvate ($\epsilon = 17.5 \text{ M}^{-1} \text{ cm}^{-1}$).
2. The colorimetric single point method²⁷. Kinetic assays (in 100 μ L total volume) were stopped by adding 11 μ L of 10% H₂SO₄ to give a final concentration of 1% H₂SO₄. The product of the enzymatic reaction, 2-acetolactate, was converted to acetoin by incubating the resultant mixture at 60°C for 15 min. The amount of acetoin was determined by incubation with 120 μ L of 0.5% creatine (w/v) and 120 μ L of 5% α -naphthol (w/v) in 4 M NaOH for 15 min at 60°C , followed by 10 min incubation on ice for colour development. The samples were then centrifuged at $9335 \times g$ rpm for two minutes to remove any precipitate. 200 μ L of the supernatant was aliquoted into a flat bottomed 96-well plate (Pathlength at 200 μ L = 0.555 cm) and the A₅₂₅ (absorbance of acetolactate at 525 nm) of the supernatant was measured ($\epsilon_M = 22,700 \text{ M}^{-1} \text{ cm}^{-1}$).

Determination of the kinetic parameters (K_{cat} and K_M) of AfuAHAS reaction. The continuous spectrophotometric method (see above) was used to determine the K_M of the substrate, pyruvate. The FAD of AfuAHAS was fully reduced to remove the lag phase prior to measuring the rates¹⁹. 100 μ L of assay mixture was incubated at 30°C at varying pyruvate concentrations (0.03–200 mM) containing 6.6 μ M AfuAHAS. The data were fitted to the Michaelis–Menten equation to obtain the K_M and the k_{cat} .

Preparation of partial anoxic buffer. Partial anoxic assay buffer was made by bubbling nitrogen gas through the standard assay buffer for 30 min to purge dissolved oxygen and by including 14.2 μ M 2-mercaptoethanol¹². The combined effect of 2-mercaptoethanol and nitrogen bubbling on accumulative inhibition generated by PS is shown in Supplementary Fig. 2.

K_i determination by the colorimetric single point method. 49.37 nM AfuAHAS was first incubated at 30°C in partial anoxic assay buffer for 20 min. Next, 90 μ L of the assay mixture containing the enzyme was added to 8 μ L of nitrogen-gas-treated water containing 2 μ L of varying concentrations of inhibitors dissolved in dimethyl sulfoxide (DMSO), including DMSO alone for the control. The mixture was then incubated at 30°C for 15 min, before stopping the reaction with 10% H₂SO₄ and quantifying the amount of 2-acetolactate (see colorimetric method above). The experiments were repeated three times. Equation (1)²⁸ was used to fit the data for tight binding inhibitors (CE and all triazolopyrimidines apart from FT) for which the enzyme concentration has to be taken into account. Equation (2)²⁹ was used to fit the data for all other herbicides (medium binding inhibitors). V_0 and V_1 are the uninhibited rate and inhibited rate respectively, $[I]$ is the total inhibitor concentration and $[E]$ is the total enzyme concentration.

$$V_1 = V_0 * \frac{-([I] - [E] + K_i) + \left(([I] - [E] + K_i)^2 + 4 * [E] * K_i \right)^{0.5}}{2 * [E]} \quad (1)$$

$$V_1 = \frac{V_0}{1 + \frac{[I]}{K_i}} + c \quad (2)$$

Accumulative inhibition assay. The continuous spectrophotometric method (see above) was used where 2.6 μ M AfuAHAS was incubated with the standard assay buffer at 30°C for 20 min to reach maximum enzyme activity before addition of inhibitor. 25 nM of PS, FS, and MT, and 100 nM of the other herbicides were used in the assay. The accumulative inhibition induced by these herbicides was observed for 45 min. All experiments were repeated three times. The data were fitted to Eq. (3)^{10,11} to calculate the kinetic rate constants k_{iapp} and k_3 (Table 1).

$$[P] = V_{max} \left(F \left(\frac{k_3}{k_{iapp} + Fk_3} \right) t + \left(\frac{k_{iapp}}{k_{iapp} + Fk_3} \right) \frac{1}{k_{iapp}/F + k_3} \left(1 - \exp \left[- \left(\frac{k_{iapp}}{F} + k_3 \right) t \right] \right) \right) \quad (3)$$

where F represents the ratio of free enzyme/enzyme-inhibitor complex. For potent inhibitors (K_i values < 100 nM, CE, PS, FS, MT, DS, PYS and CSM), the enzyme-inhibitor complex concentration is equal to the total inhibitor concentration because the K_i values are less than the concentration of the enzyme used in the assay (2.6 μ M) by more than one order of magnitude. In this case, all inhibitor molecules are bound to an enzyme. However, for inhibitors with high K_i values (> 100 nM) (ES, SM, BSM, PC and TCM), not all the inhibitor molecules are bound

to an enzyme, which has to be taken into account in the calculation of the F value. The effective concentration of enzyme-inhibitor complex was calculated using the inhibition constant formula [Eq. (4)].

$$K_i = [E][I]/[EI] \quad (4)$$

where $[E]$ represents the uninhibited enzyme concentration, $[I]$ the unbound inhibitor concentration, $[EI]$ the enzyme-inhibitor complex concentration.

Stoichiometry of enzyme inhibition. AHAS activity was monitored using the continuous method. For this study, CE was chosen as the inhibitor as it binds tightly to the enzyme and without accumulative inhibition in the presence of 2-mercaptoethanol. Increasing concentrations (2–6 μM) of *Afu*AHAS were incubated in the standard assay buffer with the addition 14.2 μM 2-mercaptoethanol for 15 min until maximum activity was reached. 0.5 μM of CE was then added and the enzyme activity for the first 200 s of inhibition was recorded to determine the initial inhibition rates without accumulative inhibition. A control without inhibitor was included and the measurements were performed in triplicates.

Fitting of the data. Fitting of data was performed using GraphPad Prism 7.01 (GraphPad Software, San Diego California USA, www.graphpad.com).

Antifungal susceptibility assays. The antifungal susceptibility assays were conducted according to Clinical and Laboratory Standards Institute guidelines for broth microdilution M32-A2³⁰, except the testing media contained Yeast Nitrogen Base, without amino acids or ammonium sulfate, buffered with 50 mM 2-[4-(2-hydroxyethyl)piperazin-1-yl]ethanesulfonic acid (HEPES), 2% glucose and 10 mM ammonium sulfate were added to the solution as the carbon and nitrogen sources, respectively. The medium was adjusted to pH 7.0 using 4 M sodium hydroxide and then stored at room temperature. 10 mg/mL stocks of each herbicide were prepared in DMSO. 10 serial twofold dilutions were conducted, giving a dilution range of 0.097656–100 $\mu\text{g/mL}$ for each antifungal agent. *A. fumigatus* strain ATCC MYAA 3626 was used in this assay. The 96-well plates were incubated at 35 °C for 48 h, and the OD_{530} of each well was recorded using the Molecular Devices Spectramax 250 microplate reader (Marshall Scientific). Each experiment was performed in triplicate.

Multiple sequence alignment. The protein sequences for the AHAS catalytic subunits were obtained from NCBI, under the accession numbers NP_013826.1 (*Sc*AHAS), NP_190425.1 (*Arabidopsis thaliana* AHAS (*At*AHAS)), EEQ44292.1 (*Ca*AHAS), AAK83371.1 (*C. neoformans* AHAS) and XP_754588.1 (*Afu*AHAS). Multiple sequence alignment was performed using T-Coffee³¹.

Molecular modelling. The homology model of *Afu*AHAS was generated using SWISS-MODEL²¹. As the herbicide binding site conformation of *Ca*AHAS is similar to that of *Afu*AHAS, binding in *Afu*AHAS was determined by superimposing the *Ca*AHAS structures in complex with the herbicides chlorimuron ethyl (CE, PDB ID 6DEL), sulfometuron methyl (SM, PDB ID 6DEP), bensulfuron methyl (BSM, PDB ID 6DEM), penoxsulam (PS, PDB ID 6DEQ), metosulam (MT, PDB ID 6DER) and propoxycarbazonone (PC, PDB ID 6DES) using Coot³². Energy minimization of these docked/superimposed structures was performed using the YASARA energy minimization server³³.

Received: 4 July 2021; Accepted: 6 October 2021

Published online: 26 October 2021

References

- Latge, J. P. *Aspergillus fumigatus* and aspergillosis. *Clin. Microbiol. Rev.* **12**, 310–350. <https://doi.org/10.1128/CMR.12.2.310> (1999).
- Kosmidis, C. & Denning, D. W. The clinical spectrum of pulmonary aspergillosis. *Thorax* **70**, 270–277. <https://doi.org/10.1136/thoraxjnl-2014-206291> (2015).
- Denning, D. W. & Perlin, D. S. Azole resistance in *Aspergillus*: A growing public health menace. *Future Microbiol.* **6**, 1229–1232. <https://doi.org/10.2217/fmb.11.118> (2011).
- Steenwyk, J. L. *et al.* Pathogenic allopolyploid hybrids of *Aspergillus* fungi. *Curr. Biol.* **30**, 2495–3250. <https://doi.org/10.1016/j.cub.2020.04.071> (2020).
- Kingsbury, J. M., Yang, Z., Ganous, T. M., Cox, G. M. & McCusker, J. H. *Cryptococcus neoformans* Ilv2p confers resistance to sulfometuron methyl and is required for survival at 37 °C and in vivo. *Microbiology* **150**, 1547–1558. <https://doi.org/10.1099/mic.0.26928-0> (2004).
- Kingsbury, J. M. & McCusker, J. H. Cytocidal amino acid starvation of *Saccharomyces cerevisiae* and *Candida albicans* acetolactate synthase (*ilv2Δ*) mutants is influenced by the carbon source and rapamycin. *Microbiology* **156**, 929–939. <https://doi.org/10.1099/mic.0.034348-0> (2010).
- Schloss, J. V., Ciskanik, L. M. & Dyk, D. E. V. Origin of the herbicide binding site of acetolactate synthase. *Nature* **331**, 360–362. <https://doi.org/10.1038/331360a0> (1988).
- Duggleby, R. G. & Pang, S. S. Acetohydroxyacid synthase. *BMB Rep.* **33**, 1 (2000).
- Gutteridge, S. *et al.* *Modern Crop Protection Compounds* 29–162 (Wiley, 2012).
- Lonhienne, T. *et al.* Structural insights into the mechanism of inhibition of AHAS by herbicides. *Proc. Natl. Acad. Sci. USA* **115**, E1945–E1954. <https://doi.org/10.1073/pnas.1714392115> (2018).
- Lonhienne, T. *et al.* Commercial herbicides can trigger the oxidative inactivation of acetohydroxyacid synthase. *Angew. Chem. Int. Ed. Engl.* **55**, 4247–4251. <https://doi.org/10.1002/anie.201511985> (2016).

12. Garcia, M. D., Nouwens, A., Lonhienne, T. G. & Guddat, L. W. Comprehensive understanding of acetohydroxyacid synthase inhibition by different herbicide families. *Proc. Natl. Acad. Sci. USA*. **114**, E1091–E1100. <https://doi.org/10.1073/pnas.1616142114> (2017).
13. Garcia, M. D. *et al.* Commercial AHAS-inhibiting herbicides are promising drug leads for the treatment of human fungal pathogenic infections. *Proc. Natl. Acad. Sci. USA*. **115**, E9649–E9658. <https://doi.org/10.1073/pnas.1809422115> (2018).
14. Lee, Y. T. *et al.* Sulfonylureas have antifungal activity and are potent inhibitors of *Candida albicans* acetohydroxyacid synthase. *J. Med. Chem.* **56**, 210–219. <https://doi.org/10.1021/jm301501k> (2013).
15. Richie, D. L. *et al.* Identification and evaluation of novel acetolactate synthase inhibitors as antifungal agents. *Antimicrob. Agents Chemother.* **57**, 2272–2280. <https://doi.org/10.1128/AAC.01809-12> (2013).
16. Pang, S. S. & Duggleby, R. G. Expression, purification, characterization, and reconstitution of the large and small subunits of yeast acetohydroxyacid synthase. *Biochemistry* **38**, 5222–5231. <https://doi.org/10.1021/bi983013m> (1999).
17. Pang, S. S., Duggleby, R. G. & Guddat, L. W. Crystal structure of yeast acetohydroxyacid synthase: A target for herbicidal inhibitors. *J. Mol. Biol.* **317**, 249–262. <https://doi.org/10.1006/jmbi.2001.5419> (2002).
18. Garcia, M. D., Wang, J. G., Lonhienne, T. & Guddat, L. W. Crystal structure of plant acetohydroxyacid synthase, the target for several commercial herbicides. *FEBS J.* **284**, 2037–2051. <https://doi.org/10.1111/febs.14102> (2017).
19. Lonhienne, T. *et al.* Structures of fungal and plant acetohydroxyacid synthases. *Nature* **586**, 317–321. <https://doi.org/10.1038/s41586-020-2514-3> (2020).
20. Lonhienne, T., Garcia, M. D., Fraser, J. A., Williams, C. M. & Guddat, L. W. The 2.0 Å X-ray structure for yeast acetohydroxyacid synthase provides new insights into its cofactor and quaternary structure requirements. *PLoS ONE* **12**, e0171443. <https://doi.org/10.1371/journal.pone.0171443> (2017).
21. Waterhouse, A. *et al.* SWISS-MODEL: Homology modelling of protein structures and complexes. *Nucleic Acids Res.* **46**, W296–W303. <https://doi.org/10.1093/nar/gky427> (2018).
22. McNicholas, S., Potterton, E., Wilson, K. S. & Noble, M. E. Presenting your structures: The CCP4mg molecular-graphics software. *Acta Crystallogr. D Biol. Crystallogr.* **67**, 386–394. <https://doi.org/10.1107/S0907444911007281> (2011).
23. Paulussen, C. *et al.* Ecology of aspergillosis: insights into the pathogenic potency of *Aspergillus fumigatus* and some other *Aspergillus* species. *Microb. Biotechnol.* **10**, 296–322. <https://doi.org/10.1111/1751-7915.12367> (2017).
24. Shishodia, S. K., Tiwari, S. & Shankar, J. Resistance mechanism and proteins in *Aspergillus* species against antifungal agents. *Mycology* **10**, 151–165. <https://doi.org/10.1080/21501203.2019.1574927> (2019).
25. Subashchandrabose, S. *et al.* Branched-chain amino acids are required for the survival and virulence of *Actinobacillus pleuropneumoniae* in swine. *Infect. Immun.* **77**, 4925–4933. <https://doi.org/10.1128/IAI.00671-09> (2009).
26. Schloss, J. V., Van Dyk, D. E., Vasta, J. F. & Kutny, R. M. Purification and properties of *Salmonella typhimurium* acetolactate synthase isozyme II from *Escherichia coli* HB101/pDU9. *Biochemistry* **24**, 4952–4959. <https://doi.org/10.1021/bi00339a034> (2002).
27. Singh, B. K., Stidham, M. A. & Shaner, D. L. Assay of acetohydroxyacid synthase. *Anal. Biochem.* **171**, 173–179. [https://doi.org/10.1016/0003-2697\(88\)90139](https://doi.org/10.1016/0003-2697(88)90139) (1988).
28. Chang, A. K. & Duggleby, R. G. Expression, purification and characterization of *Arabidopsis thaliana* acetohydroxyacid synthase. *Biochem. J.* **327**(Pt 1), 161–169. <https://doi.org/10.1042/bj3270161> (1997).
29. Chang, A. K. & Duggleby, R. G. Herbicide-resistant forms of *Arabidopsis thaliana* acetohydroxyacid synthase: Characterization of the catalytic properties and sensitivity to inhibitors of four defined mutants. *Biochem. J.* **333**, 765–777 (1998).
30. CLSI. *Reference Method for Broth Dilution Antifungal Susceptibility Testing of Filamentous Fungi; Approved Standard: Second Edition.* (M28-A2 Clinical and Laboratory Standards Institute, 2008).
31. Notredame, C., Higgins, D. G. & Heringa, J. T-Coffee: A novel method for fast and accurate multiple sequence alignment. *J. Mol. Biol.* **302**, 205–217. <https://doi.org/10.1006/jmbi.2000.4042> (2000).
32. Emsley, P., Lohkamp, B., Scott, W. G. & Cowtan, K. Features and development of Coot. *Acta Crystallogr. D Biol. Crystallogr.* **66**, 486–501. <https://doi.org/10.1107/S0907444910007493> (2010).
33. Krieger, E. *et al.* Improving physical realism, stereochemistry, and side-chain accuracy in homology modeling: Four approaches that performed well in CASP8. *Proteins* **77**(Suppl 9), 114–122. <https://doi.org/10.1002/prot.22570> (2009).

Author contributions

Y.S.L., M.D.G. and T.L. performed all of the experiments. Y.S.L. wrote the first draft of the manuscript and prepared all of the figures. T.L., G.S., J.A.F. and L.W.G. provided supervision to Y.S.L. and M.D.G. and contributed to the design of experiments and planning of the manuscript. T.L., G.S., J.A.F. and L.W.G. also contributed to writing in group writing sessions and each provided individual feedback on six preliminary versions of the manuscript. L.W.G. provided overall leadership on the project leading to the submission.

Competing interests

The authors declare no competing interests.

Additional information

Supplementary Information The online version contains supplementary material available at <https://doi.org/10.1038/s41598-021-00349-9>.

Correspondence and requests for materials should be addressed to L.W.G.

Reprints and permissions information is available at www.nature.com/reprints.

Publisher's note Springer Nature remains neutral with regard to jurisdictional claims in published maps and institutional affiliations.



Open Access This article is licensed under a Creative Commons Attribution 4.0 International License, which permits use, sharing, adaptation, distribution and reproduction in any medium or format, as long as you give appropriate credit to the original author(s) and the source, provide a link to the Creative Commons licence, and indicate if changes were made. The images or other third party material in this article are included in the article's Creative Commons licence, unless indicated otherwise in a credit line to the material. If material is not included in the article's Creative Commons licence and your intended use is not permitted by statutory regulation or exceeds the permitted use, you will need to obtain permission directly from the copyright holder. To view a copy of this licence, visit <http://creativecommons.org/licenses/by/4.0/>.

© The Author(s) 2021